Long wave instability of aircraft wake vortex under shear crosswind

Ziming Xu[1], Dong Li[1], Jinyan Cai[1,2], & Jiayu Han[1]

[1]School of Aeronautics, Northwestern Polytechnical University, Xi'an, People's Republic of China
[2]China Aerodynamics Research and Development Center, Mianyang, People's Republic of China

Abstract

To a large extent, dynamic instabilities dominate the lifespan of aircraft wake vortices, which is one of the most important factors that determine the flight separation. Considering that the wake vortex instability might be affected by crosswind, the long-wave instability of the aircraft wake vortex under shear crosswind condition is investigated using linear stability analysis method for the first time. It is found that the growth rate of the long-wave instability is reduced under the influence of the strain field exerted by the crosswind shear, and the vortex filaments are inclined additionally along the crosswind speed gradient. Furthermore, the curvature corrected vortex filament method is adopted to simulate the dynamic instability. The numerical experiment results agree well with the theoretical prediction.

Keywords: aircraft wake vortex, crosswind, instability, vortex filament method

1. Introduction

The wake generated by the aircraft threatens the flight safety of the following aircraft seriously. After entering the wake area of the preceding one, the pressure distribution of the following aircraft will change dramatically, resulting in sudden lift loss and uncontrollable rolling[1, 2]. Especially, in take-off and approaching phases, the flight paths of different aircrafts are highly coincident, leading to increased possibility of wake encounters. Therefore, it is necessary to study the formation and evolution of aircraft wake carefully.

Existing studies reveal that the aircraft wake is dominated by a pair of counter-rotating vortices (wake vortex), which is the primary study objects of various relevant researches. Aircraft wake vortex decay generally contains two phases: diffusion phase and rapid decay phase[3-5]. In the diffusion phase, the decay of the vortices is dominated by viscous and turbulent diffusion. As the vorticity diffuses along the radial direction gradually, the vortex circulation (strength) decrease slowly. In the rapid decay stage, the vortex pair deforms on a large scale, and the vortex circulation rapidly decline to the extent that it is harmless to the following aircraft. Dynamic instabilities are the main mechanisms that promote the rapid decay of the wake vortex, among which, in the medium and weak intensity atmospheric turbulence (generally treated as homogeneous isotropic turbulence, HIT), long-wave instability plays a dominant role. Crow first investigated the instability of a counterrotating vortex pair with linear stability analysis method[6, 7]. It was found that the most unstable long-wave instability corresponds to a wavelength of about $8b_0$. At the same time, the two vortices are sinusoidal deformed in the fixed plane and inclined to the symmetric plane by about 45 degrees. Besides, the two vortices are connected at the closest position, causing the rapid decay phase of the wake vortex pair to begin (Figure 1). This phenomenon, known as Crow instability, has been confirmed by numerous observations in flight, experiments, and numerical simulations[8-10].

Initial disturbance and external exerted strain field are the two necessary factors to trigger the Crow instability. For wake vortex immersed in homogeneous isotropic turbulence, the initial disturbance is provided by the background turbulence field. The strain field is provided by mutual induction of the vortex pair[7, 11]. For example, the strain field experienced by the portside vortex is exactly the shear field induced by the starboard vortex. However, if the average shear of the background field is not

zero, additional strain field will be experienced by the wake vortex, and the instability parameter will be altered, which has been rarely studied.

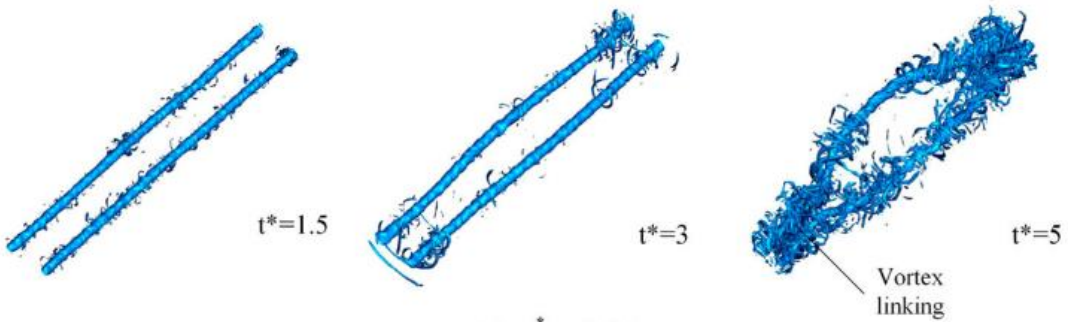

Figure 1 Crow instability under moderate turbulence[5]

In this paper, the shear crosswind effects on wake vortex instability is investigated using linear stability analysis method for the first time. And the curvature corrected vortex filament method is adopted to verify the theoretical prediction. It is found that the shear crosswind reduces the growth rate of the instability amplitude, and causes the planes where the vortex filaments lie in to tilt along the velocity gradient. The numerical results are in good agreement with the predicted values. These conclusions could work as a reference for flight interval reduction.

2. Linear stability analysis

The linear stability analysis follows Crow's method[7]. According to the vorticity transport equation and supposing non-viscous fluid, the wake vortex filament moves with the fluid particles, and the mathematical expression for the vortex is as follows:

$$\frac{\partial \mathbf{r}_n}{\partial t} + u_n \frac{\partial \mathbf{r}_n}{\partial x_\mathrm{n}} = \mathrm{e}_y v_n + \mathrm{e}_z w_n \qquad (1)$$

where $\mathbf{r}_n$ is the arbitrary radial displacement on the vortex filament, u_n, v_n, and w_n are the components of convection velocity with respect to the downward moving coordinates. e_y and e_z are the lateral and vertical unit vector, respectively. Since the axial induced velocity is small, its product with the perturbation rate of change (second term on the left of equation 1) is a second-order small quantity, which can be omitted. Therefore, in the reference frame of downward moving coordinates with ω_0(vortex pair induced velocity), equation (1) is further simplified as

$$\frac{\partial \mathbf{r}_n}{\partial t} = \mathrm{e}_y v_n + \mathrm{e}_z w_n \qquad (2)$$

The arbitrary radial displacement $\mathbf{r}_n$ could be written in Fourier series form as:

$$\mathbf{r}_n = \hat{\mathbf{r}}_n e^{\sigma t + ik\kappa_n} \qquad (3)$$

where σ is the complex growth rate and k is the disturbance wave number, respectively. To simplify the analysis, consider a constant gradient of the shear crosswind. In equation 2, v_n consists of the induced velocity of the wake vortex ($v_{n,\mathrm{induce}}$) and the crosswind velocity ($v_{n,\mathrm{crosswind}}$). Define the crosswind velocity at the height of the vortex core as v_{core}, and the crosswind gradient as k_{wind}. From the above discussion, it is clear that the whole wake vortex coordinate system is translating along the crosswind direction at the velocity of v_{core}, which does not affect the dynamic stability. Consequently, without loss of generality, v_{core} could be set to zero. In the z direction, the coordinate system is translated downward at a velocity of ω_0, and only the displacement disturbance $\hat{\mathbf{z}}_n$ will affect the wind speed felt by the local vortex. Thus, the wake vortex system as shown in Figure 2 can be obtained, or written in Fourier series form as follows:

$$\begin{aligned} v_n &= v_{n,\mathrm{induce}} + v_{n,\mathrm{crosswind}} \\ &= v_{n,\mathrm{induce}} + k_{wind} \cdot \mathrm{z}_n \\ &= v_{n,\mathrm{induce}} + k_{wind} \cdot \hat{\mathrm{z}}_n e^{\sigma t + i\kappa \mathrm{x}_n} \end{aligned} \qquad (4)$$

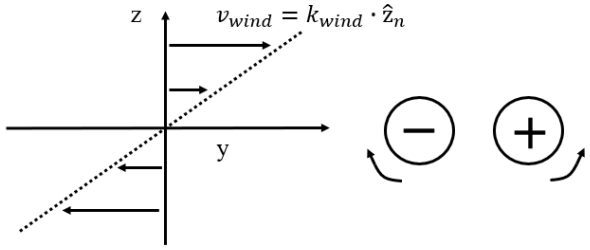

Figure 2 Velocity distribution of vortex pair and crosswind

Expand equation 4 and take the real part of equation 4 into the linear stability analysis equations (equation 8 in reference [7]), the wake vortex dynamic can be described as:

$$\begin{aligned} \alpha\hat{y}_1 &= -(1-\hat{k})\hat{z}_1 + \psi\hat{z}_2 - \beta^2\omega\hat{z}_1 \\ \alpha\hat{z}_1 &= -\hat{y}_1 + \chi\hat{y}_2 + \beta^2\omega\hat{y}_1 \\ \alpha\hat{y}_2 &= \quad (1+\hat{k})\hat{z}_2 - \psi\hat{z}_1 + \beta^2\omega\hat{z}_2 \\ \alpha\hat{z}_2 &= \quad \hat{y}_2 - \chi\hat{y}_1 - \beta^2\omega\hat{y}_2 \end{aligned} \tag{5}$$

where $\hat{y}$ and $\hat{z}$ are the amplitudes; α is the nondimensional instability growth rate, β is the nondimensional wave number. ψ and χ are composed of modified Bessel functions; $\chi(\beta) = \beta K_1(\beta)$, $\psi(\beta) = \beta^2 K_0(\beta) + \beta K_1(\beta)$. $\hat{k} = k_{wind} \cdot 2\pi {b_0}^2/\Gamma$ is the nondimensional wind gradient.

After the crosswind shear is coupled into the equations through random perturbations, the crosswind velocity gradient appears as a new coefficient in the first column on the right side of the equation 5. The crosswind shear provides an additional strain field, which essentially plays a similar role as the vortex-induced strain. In addition, it should be noted that $\hat{k}$ has the different sign as the strain field felt by the original vortex pair at $\hat{z}_1$, but the same sign as the original strain field at $\hat{z}_2$, which results in the equation being no longer symmetric, and correspondingly, the development of the vortex pair will be no longer symmetric.

3. Curvature corrected vortex filament method

3.1 Numerical discretization schemes

The Vortex Filament Method (VFM) is widely used to simulate helicopter wakes and wind turbine wakes[12]. The wake vorticity field is simplified as several vortex filaments with radius equaling to zero. And vortex circulation remain constant along each filament. Similarly, the characteristics and development of aircraft wake vortex pair can also be well described by vortex filaments. With incompressible and non-viscous assumption, the governing equation (vorticity equation) under the Lagrange perspective can be written as:

$$\frac{d\boldsymbol{S}}{dt} = \boldsymbol{V}, \boldsymbol{S}(t=0) = \boldsymbol{S}_0 \quad (6)$$

where $\boldsymbol{S}$ is the position of an arbitrary control point in the filament, $\boldsymbol{S}_0$ is the initial position of the point, and $\boldsymbol{V}(\boldsymbol{S})$ is the velocity vector. With the initial vorticity distribution prescribed, evolution of the flow field can be advanced by equation(6).

During the simulation, each vortex filament is discrete into n vortex elements with both ends as control points (Figure 3). And the induced velocity on an arbitrary point p is

$$\boldsymbol{V}_p = \sum_{i=1}^{n} \boldsymbol{V}_{l_i p} \quad (7)$$

$$\boldsymbol{V}_{l_i p} = \frac{\Gamma}{4\pi} \int \frac{d\boldsymbol{l} \times \boldsymbol{q}}{(|\boldsymbol{q}|^2 + a r_c^2)^{3/2}} \quad (8)$$

where Γ is the vortex filament circulation, $d\boldsymbol{l}$ is the differential of element l_i, $\boldsymbol{q}$ is the vector from point p to element l_i, r_c is the vortex radius. a equals to 0.2065.

For traditional VFM simulations, the vortex elements are treated as straight ones. And each element exert zero induced velocity on itself. Take element l_i in Figure 3 as an example, the induction velocity of l_i on control points N_i is:

$$\boldsymbol{V}_{l_i,N_i} = \frac{\Gamma}{4\pi}\int \frac{\mathrm{d}\boldsymbol{l}\times\boldsymbol{q}}{(|\boldsymbol{q}|^2+ar_c^2)^{3/2}} = 0, \boldsymbol{q} = 0 \qquad (9)$$

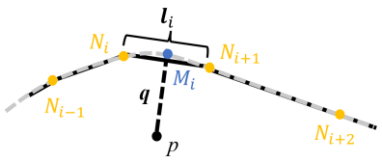

Figure 3 Discretization of vortex filament

thus producing inaccurate solution of vorticity distribution. In recent works[13], the curvature corrected VFM (CCVFM) was developed by considering the vortex element as curved ones. The coordinate of M_i (midpoint of element l_i) is firstly obtained by cubic spline interpolation. Then, the induced velocity of element l_i on N_i is:

$$\boldsymbol{V}_{l_i,N_i} = \frac{\Gamma}{4\pi}\left(\frac{\mathrm{d}\boldsymbol{l}_{N_i}\times\boldsymbol{q}_{N_i,N_i}}{(\left|\boldsymbol{q}_{N_i,N_i}\right|^2+ar_c^2)^{3/2}} + 4\frac{\mathrm{d}\boldsymbol{l}_{M_i}\times\boldsymbol{q}_{M_i,N_i}}{(\left|\boldsymbol{q}_{M_i,N_i}\right|^2+ar_c^2)^{3/2}} + \frac{\mathrm{d}\boldsymbol{l}_{N_{i+1}}\times\boldsymbol{q}_{N_{i+1},N_i}}{(\left|\boldsymbol{q}_{N_{i+1},N_i}\right|^2+ar_c^2)^{3/2}}\right) \qquad (10)$$

In equation (10), the trapezoidal integral formula is adopted to perform the integration of equation (8).

3.2 Method validation

Aircraft wake vortex pair could be described by three parameters, initial vortex spacing (b_0), initial core radius (r_c), and initial circulation (Γ_0). For wake vortex generated by elliptical loaded wing, r_c/b_0 equals to 0.0981. And the most unstable wave length is $8.607b_0$, with $\alpha = 0.827$ (nondimensional amplitude growth rate) and $\theta = 48^\circ$ (vortex filament inclination angle). In this paper, the wake vortex of an A340 aircraft is modeled, the characteristic parameters are listed in Table 1.

Table 1 Characteristic parameters of A340 wake vortex pair

Parameter	Value
Γ_0	$460\mathrm{m}^2/\mathrm{s}$
b_0	$47.4\mathrm{m}$
r_c	$4.65\mathrm{m}$
ω_0=$\Gamma_0/2\pi b_0$ (characteristic velocity)	$1.54\mathrm{m/s}$
t_0=b_0/ω_0 (characteristic time)	$30.69\mathrm{s}$

To validate the accuracy of CCVFM method, the evolution of A340 wake vortex pair is simulated. To trigger the long wave instability, a sinusoidal disturbance is imposed on the vortex filament. The disturbance has a wavelength of $8.607b_0$. The spanwise and vertical amplitude of the disturbance are $R_{y,0} = R_{z,0} = 0.0084b_0$. The total amplitude of the vortex filament is:

$$R_A = \sqrt{{R_y}^2 + {R_z}^2} \qquad (11)$$

Different timesteps (Δt) and vortex element numbers (n) are tested as listed in Table 2.

Table 2 Case settings for method validation

Case	n	$\Delta t/t_0$
1	25	3.26×10^{-3}
2	50	3.26×10^{-3}
3	100	3.26×10^{-3}
4	200	3.26×10^{-3}
5	50	1.63×10^{-3}
6	50	6.52×10^{-3}
7	50	16.2×10^{-3}

Figure 4 and Figure 5 exhibit the wake vortex evolution with different discretization settings. It is

observed that employing 50 elements on each filament and $\Delta t/t_0 = 3.26 \times 10^{-3}$ is sufficient to model the instability accurately. Both the amplitude growth rate and vortex inclination angel agree with the theoretical prediction well. In subsequent sections, $n = 100$ and $\Delta t/t_0 = 3.26 \times 10^{-3}$ are employed to assure the simulation accuracy.

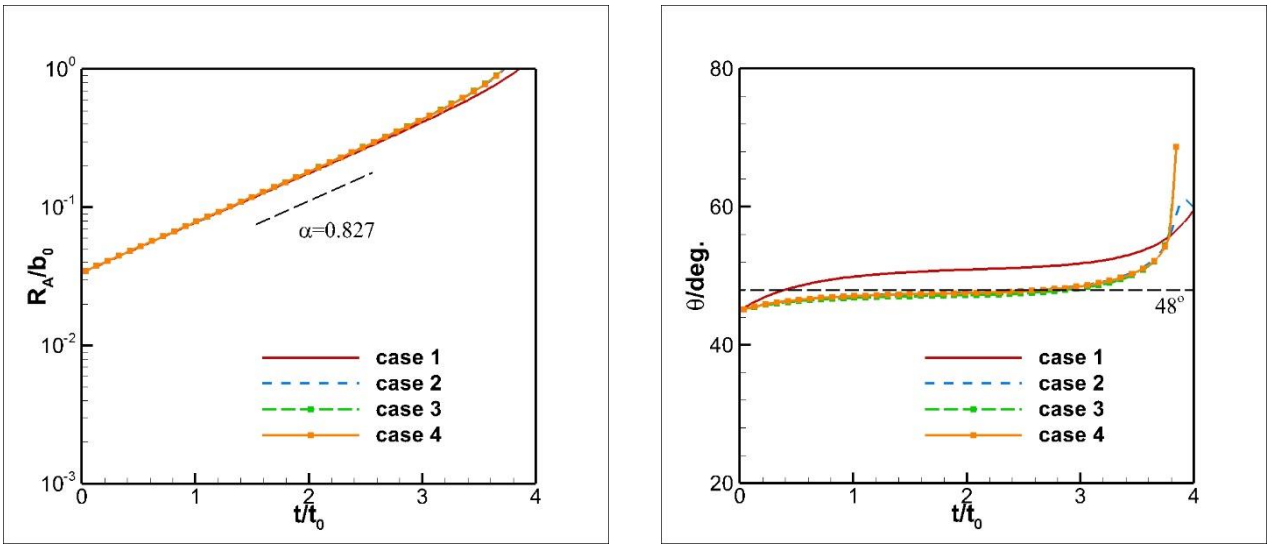

a. Amplitude growth history b. Inclination history

Figure 4 Evolution of vortex pair with different element numbers

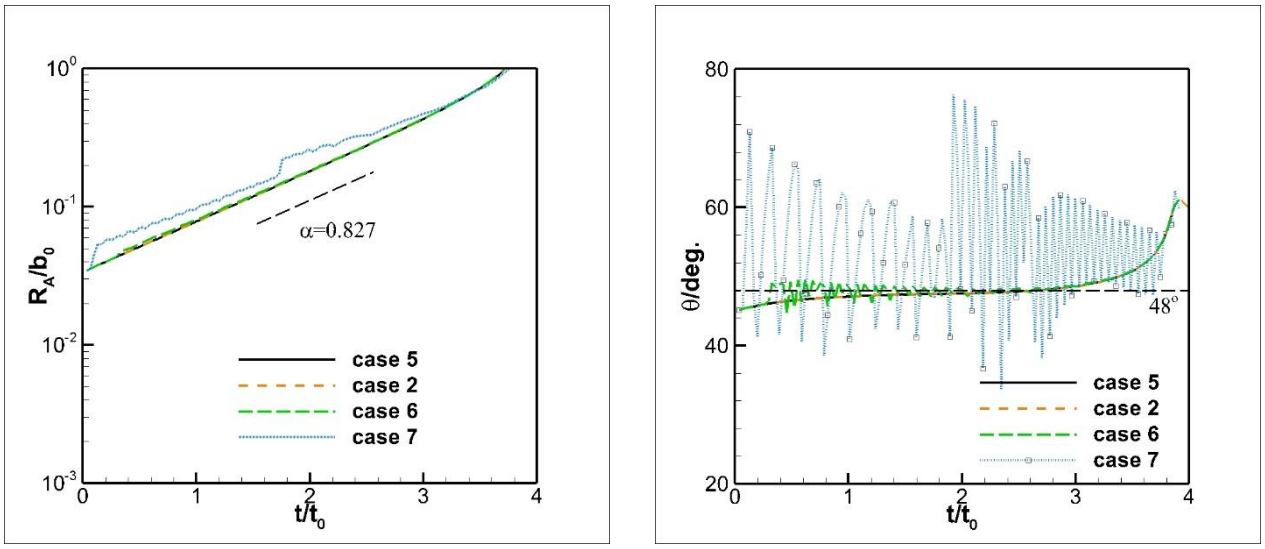

a. Amplitude growth history b. Inclination history

Figure 5 Evolution of vortex pair with different timesteps

4. Instability of wake vortex under shear crosswind condition

4.1 Theoretical prediction

In this section, a crosswind gradient of $k = 0.03/s$ is considered. With the wake vortex parameters of $b_0 = 47.4\text{m}$ and $\Gamma_0 = 460\text{m}^2/s$, the corresponding nondimensional wind gradient value is $\hat{k} = 0.92$.

Figure 6 shows the instability predicted by the linear stability analysis. Here, the two vortices are distinguished according to the vorticity carried by the crosswind. The vortex containing the same sign vorticity as the crosswind field vorticity is vortex 1, and the other vortex is vortex 2. Taking Figure 2 as an example, the crosswind vorticity is negative, so the left vortex is vortex 1, and the right vortex is vortex 2. As shown in Figure 6a, comparing to the no-wind case, the shear crosswind with $\hat{k} = 0.92$ reduces the instability growth rate to a large extent. And as disturbance wave number increases, the disturbance wavelength becomes shorter, and the growth rate difference between the no-wind case and the shear wind case gradually decreases. When nondimensional disturbance wave number approaches 1.1, the amplitude growth rate curves in the two cases almost coincide. In addition, shear

crosswind has significant influence on the inclination of vortex filaments. Figure 6b shows that with $\beta < 0.577$, both vortices tilt along the crosswind gradient direction.

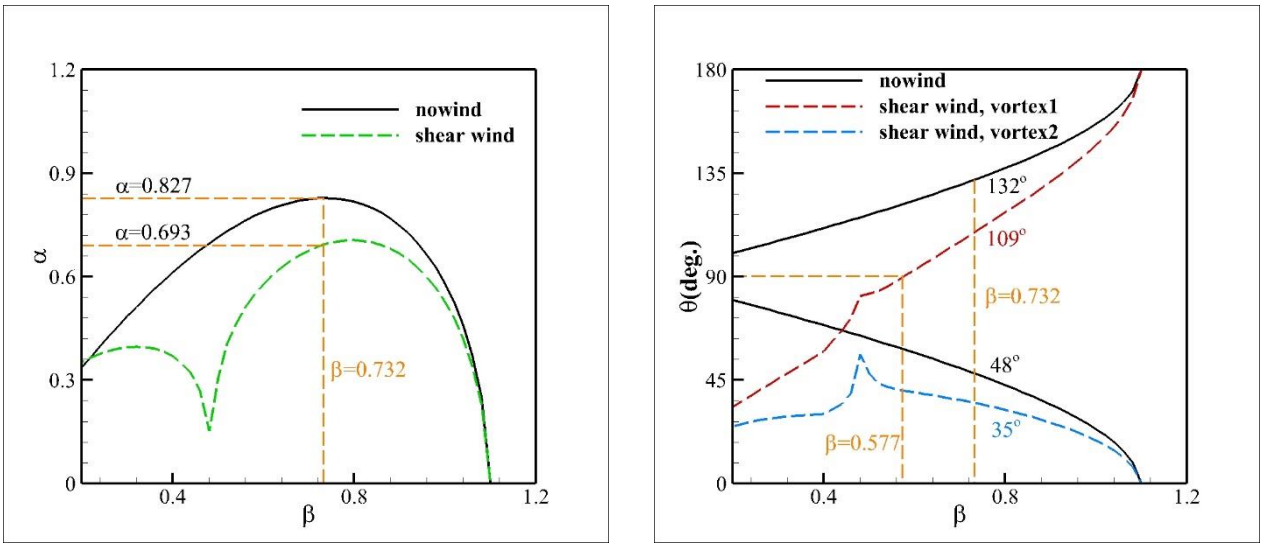

a. Nondimensional amplitude growth rate vs. nondimensional wave number

b. Vortex filament incline angle vs. nondimensional wave number

Figure 6 Instability predicted by linear stability analysis

4.2 CCVFM simulation result

Figure 7 shows the 3D structures of vortex pair when $\hat{k} = 0$ (no-wind case, red) and $\hat{k} = 0.92$ (shear wind case, blue). Although the initial conditions of the two cases are the same, the inclination angle of the vortices are obviously different at $t^* = 1$. In the shear wind case, the plane where the two vortices are located has a clockwise deflection compared with the no-wind case. At $t^* = 4$, the vortex filaments in the no-wind case develops symmetrically, and the vortex linking has occurred at the closest position of the spacing of filaments, while in the crosswind case, the distance between the two vortex filaments is still large.

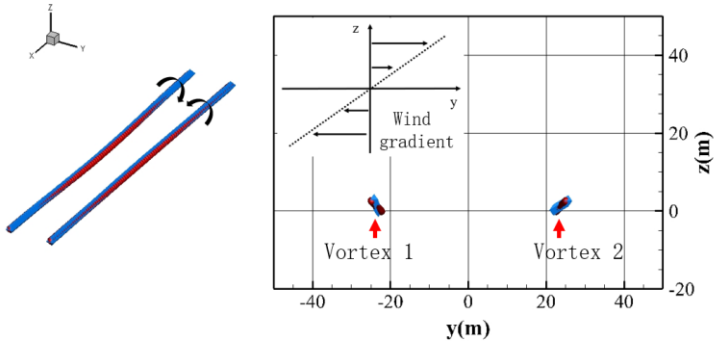

a. $t^* = 1$

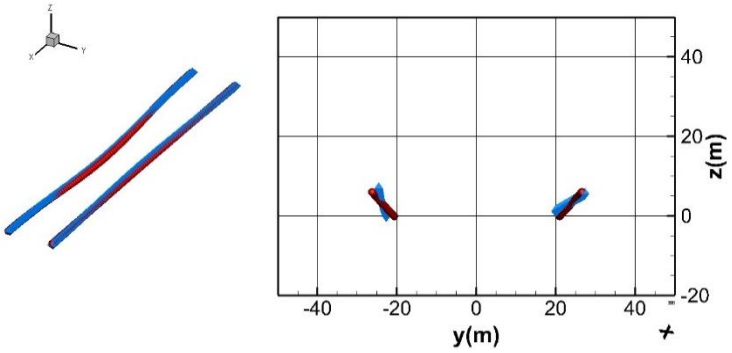

b. $t^* = 2$

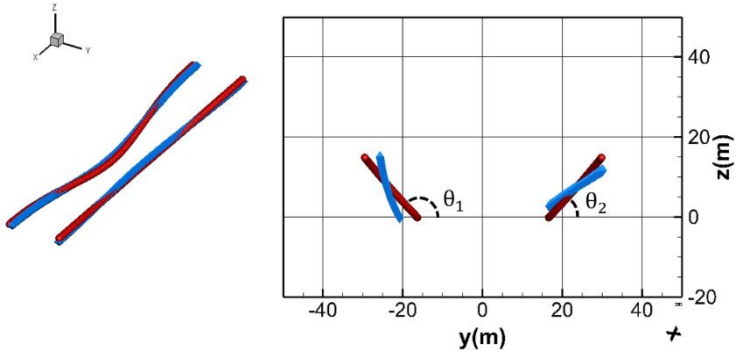

c. $t^* = 3$

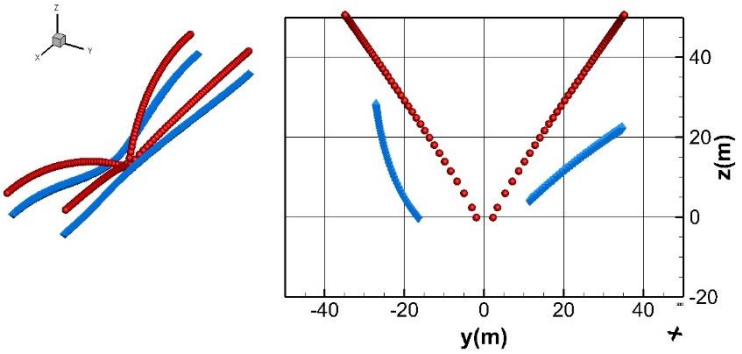

d. $t^* = 4$

Figure 7 vortex structures development predicted by vortex filament method

Figure 8 shows the development of wake vortex instability under no-wind case and shear wind case with a nondimensional wave number of $\beta = 0.7332$. The instability growth rate of the two vortices in the crosswind case were inconsistent in the initial stage, but both remained 0.693 in the linear growth stage. $\alpha = 0.693$ was significantly lower than the growth rate in the no-wind case ($\alpha = 0.827$), which was consistent with the prediction of the aforementioned stability analysis in Figure 6. In addition, the inclination of the two vortices driven by crosswind changes, and the inclination trend is related to the wind gradient. However, it should be noted that the instability of the wake vortex is a dynamic process, and the inclination angle also changes dynamically with the deformation of the filament. But in general, the inclination angle is close to the prediction in Figure 6b.

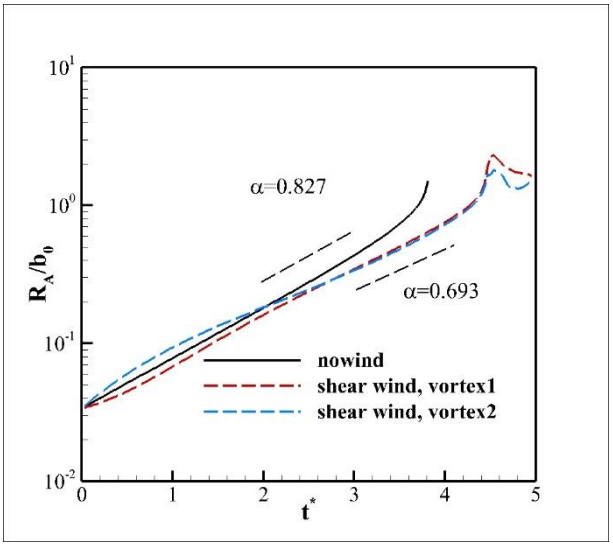

a. Amplitude of vortex filaments

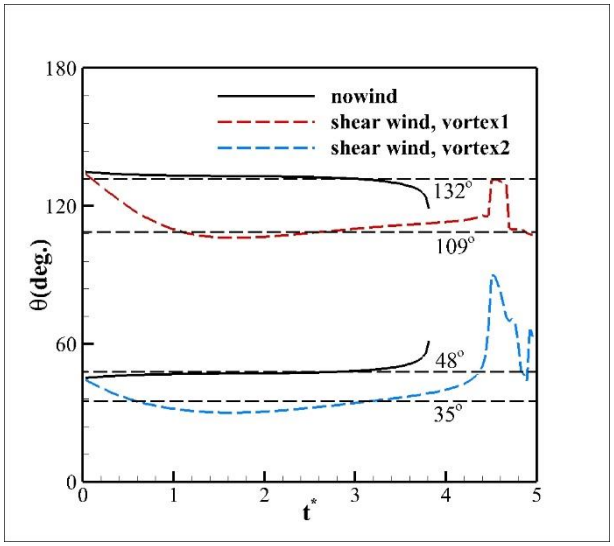

b. Inclination of vortex filaments

Figure 8 Instability simulated by the vortex filament method

5. Conclusion

In this paper, the long-wave instability of the aircraft wake vortex pair under crosswind condition is

deduced using linear stability analysis method. By considering the crosswind component, the influence of the crosswind shear on the vortex instability is analyzed in this paper and verified using the curvature corrected vortex filament method (CCVFM). Theoretical analysis and numerical experiments demonstrate that the shear crosswinds will have a significant effect on the dynamic destabilization process of the wake vortex pair. It is found that the growth rate of the long-wave instability amplitude will be reduced under the influence of the strain field brought by the shear crosswind, and the vortex filaments will be inclined additionally along the crosswind speed gradient.

Contact Author Email Address

Contact author: Dong Li, ldgh@nwpu.edu.cn

Copyright Statement

The authors confirm that they, and/or their company or organization, hold copyright on all of the original material included in this paper. The authors also confirm that they have obtained permission, from the copyright holder of any third party material included in this paper, to publish it as part of their paper. The authors confirm that they give permission, or have obtained permission from the copyright holder of this paper, for the publication and distribution of this paper as part of the ICAS proceedings or as individual off-prints from the proceedings.

References

[1] Hallock J N, Holzäpfel F. A review of recent wake vortex research for increasing airport capacity[J]. *Progress in Aerospace Sciences*, 2018,98:27-36.

[2] Gerz T, Holzäpfel F, Darracq D. Commercial aircraft wake vortices[J]. *Progress in Aerospace Sciences*, 2002,38(3):181-208.

[3] Hennemann I, Holzäpfel F. Large-Eddy simulation of aircraft wake vortex deformation and topology[J]. *Proceedings of the Institution of Mechanical Engineers, Part G: Journal of Aerospace Engineering*, 2011,225(12):1336-1350.

[4] Xu Z, Li D, Cai J. Long-wave deformation of in-ground-effect wake vortex under crosswind condition[J]. *Aerospace Science and Technology*, 2023,142:108697.

[5] Zhou J, Chen Y, Li D, et al. Numerical simulation of aircraft wake vortex evolution and wake encounters based on adaptive mesh method[J]. *Engineering Applications of Computational Fluid Mechanics*, 2020.

[6] Crow S C, Bate E R. Lifespan of trailing vortices in a turbulent atmosphere[J]. *Journal of Aircraft*, 1976,13(7):476-482.

[7] Crow S C. Stability Theory for a Pair of Trailing Vortices[J]. *AIAA Journal*, 1970.

[8] Lin M, Cui G, Zhang Z. Large eddy simulation of aircraft wake vortex with self-adaptive grid method[J]. *Applied Mathematics and Mechanics-English Edition*, 2016,37(10).

[9] Zhou J, Li D, Zhang Z, et al. Numerical Simulation of Energy Distribution of Turbulent Vortices in Atmosphere Effects on Aircraft Wake Vortices[J]. *Journal of Physics. Conference Series*, 2021,1828(1):12167.

[10] Misaka T, Holzäpfel F, Hennemann I, et al. Vortex bursting and tracer transport of a counter-rotating vortex pair[J]. *Physics of Fluids*, 2012,24(2):25104.

[11] Bristol R L. Cooperative wake vortex instability[D]. *University of California at Berkeley*, 2000.

[12] Leishman J G, Bhagwat M J, Bagai A. Free-Vortex Filament Methods for the Analysis of Helicopter Rotor Wakes[J]. *Journal of Aircraft*, 2002,39(5).

[13] Xu Z, Li D, Cai J, et al. Fast simulation method for three dimensional instability of an aircraft wake vortex pair[J]. *Acta Aerodynamica Sinica*, 2023.